NICST Internal Memo

Date: June 19, 2008
From: J McIntire, C. Pan, and S. Xiong
To: Bruce Guenther, Jim Butler, Jack Xiong
Subject: Updated Analysis of the Radiometric Calibration from the VIIRS EDU RC-05 Part 2 Test (Nominal Plateau at 28V)

References:

[1] NICST_MEMO_08_024, "Updated Analysis Results for VIIRS EDU RC-05 Part 1, Nominal Plateau at 28V," J. McIntire, C. Pan, and S. Xiong, July 1, 2008.
[2] NICST_MEMO_08_025, "Sensitivity of the VIIRS Sensor Determined from the EDU RC-05 Part 1 test (Nominal Plateau at 28V)," J. McIntire, C. Pan, and S. Xiong, July 8, 2008.
[3] NICST_REPORT_06_009, 'Preliminary test analysis report of VIIRS EDU RC-05 Parts 1 & 2 in TV at Nominal Plateau,' August 4, 2006.
[4] NICST_REPORT_06_025, 'Radiometric Characterization Report of EDU RC-05 Part1 Using BCS at Hot Plateau (28V) and Comparison with Cold & Nominal,' December 13, 2006.
[5] Y18352, 'Performance Verification Review: Thermal Emissive Band Radiometric response Characterization (RC-3 and RC-5 Tests),' Eric Johnson and Jim Young, January 18, 2006.
[6] 'Sensor Performance Verification Plan,' PVP154640-101.
[7] 'Performance Specification Sensor Specification,' ps154640-101c.

1. Introduction

The VIIRS EDU thermal vacuum test RC-05 Part 2 was designed to examine the sensor response to the On-Board Calibration (OBC) blackbody in a near space-like environment. NICST analysis results for the nominal plateau portion of this test (both Parts 1 and 2) were reported for the radiometric gains and sensitivity as well as for compliance with a number of specifications [1-4]. This work will focus on the warm-up and cool-down (RC-05 Part 2) radiometric gains for the nominal plateau at 28V, as an update to previous work [3].

Table 1 lists the relevant UAIDs along with their corresponding OBC and Blackbody Calibration Source (BCS) temperatures (the collect label defines the order in which they were analyzed). Each collect contains 100 scans. This test consisted of two parts: warm-up and cool-down of the OBC temperature. The warm-up portion (UAIDs 2002542-3) was conducted with the OBC temperature controlled over all scans in each collect. For the cool-down (UAID 2002544) segment of this test, the OBC temperature was set at the beginning of each collect and then allowed to drift over scans. The BCS source was

located in the last collect window. In addition, the Space View Source (SVS) was positioned in the Space View (SV) port. Band M13 in low gain mode was not considered. The VIIRS sensor was operated in diagnostic mode. The general outline of the methodology used in this work follows from [1,5,6] with some modifications.

2. Data Processing

The VIIRS EDU TV tests were conducted using the F9 apeture. However, all of the specifications for the VIIRS sensor assume a F6 apeture. In order to convert the radiance for comparison to the F9 specifications, the following factor was employed:

$$L_{F6} = L_{F9}\left(\frac{6}{9}\right)^2 . \quad (1)$$

Notice that it is the radiances, and not the temperatures, that are rescaled.

All the samples for both the OBC and SV were analyzed. The BCS data analyzed here is restricted to a subset of the Earth View (EV) samples in a given collect for which the BCS source yielded a stable response (the sweetspot). The following sample ranges were used in this work: samples 1650 – 1849 for M bands and samples 3300 – 3699 for I bands. Note that the BCS data was only used to calculate the retrieved OBC radiance.

The response was analyzed using the scan method. First, the DN_{SV} was averaged over all samples in a given scan. Then, $<DN_{SV}>_{samples}$ was subtracted from each sample of the DN_{OBC}. Next, the dn was averaged over samples, or $<dn>_{samples}$. The standard deviation of all samples for a specific scan was calculated, or $\sigma_{samples}$. Note that the HAM sides alternate from scan to scan such that there are 50 scans for each HAM side. Additionally, for this memo the I band data is divided into two subsamples where the larger for both SV and OBC is always labeled subsample 1, to ensure the proper background subtraction. The same treatment was used for the EV data.

The temperatures (T_{xxx}) of the following were extracted: OBC, BCS, SVS, HAM, and Rotating Telescope Assembly (RTA). The OBC, HAM, and RTA temperatures were acquired using the LRV extractor and the BCS and SVS temperatures were obtained from the GSE files.

For each of these temperatures, a Planck radiation was calculated using the center wavelength (λ) of each band and the equation

$$L_{xxx}(\lambda, T_{xxx}) = \frac{2hc}{\lambda^5}\frac{1}{e^{hc/\lambda k T_{xxx}} - 1} . \quad (2)$$

Then, the in-band Relative Spectral Response (RSR) was applied as a correction to the Planck radiances; this was implemented by the following equation

$$\langle L_{xxx}(B, D, j_H, T_{xxx}) \rangle = \frac{\int RSR(B, D, \lambda)\, L_{xxx}(B, j_H, T_{xxx})\, d\lambda}{\int RSR(B, D, \lambda)\, d\lambda}, \quad (3)$$

where B, D, and j_H represent band, detector, and scan (HAM side dependent), respectively. The RSR data was available for only some detectors; therefore, the existing

RSR was extrapolated to the missing detectors. The RSR used here was calculated by the NICST team.

The effective OBC radiance is

$$\begin{aligned}\left\langle L_{OBC}\left|B,D,j_H,T_{OBC}\right.\right\rangle_{eff} &= \varepsilon_{OBC}\left\langle L_{OBC}\left|B,D,j_H,T_{OBC}\right.\right\rangle \\ &-\left(1-\varepsilon_{OBC}\right)\left[F_{CAV}\left\langle L_{CAV}\left|B,D,j_H,T_{OBC}\right.\right\rangle\right. \\ &+F_{SH}\left\langle L_{SH}\left|B,D,j_H,T_{OBC}\right.\right\rangle \\ &\left.+F_{RTA}\left\langle L_{RTA}\left|B,D,j_H,T_{OBC}\right.\right\rangle\right]\end{aligned}, \tag{4}$$

where ε_{OBC} is the emissivity of the OBC and F_{CAV}, F_{SH}, and F_{RTA} are the fraction of the OBC reflectance attributable to the scan cavity (CAV), RTA, and OBC shield (SH), respectivily.

The PVP defines the background radiance as

$$\begin{aligned}\left\langle L_{Bkg}\left|B,D,j_H,T_{OBC}\right.\right\rangle &= rvs\left(B,\phi_{SVS},H\right)\left\langle L_{SVS}\left|B,D,T_{OBC}\right.\right\rangle \\ &-\frac{rvs\left(B,\phi_{SVS},H\right)-rvs\left(B,\phi_{xxx},H\right)}{\rho_{RTA}\left(B\right)} \\ &\times\left\langle L_{HAM}\left|B,D,j_H,T_{OBC}\right.\right\rangle-\left(1-\rho_{RTA}\left(B\right)\right)\left\langle L_{RTA}\left|B,D,j_H,T_{OBC}\right.\right\rangle\end{aligned} \tag{5}$$

This includes contributions from not only the SVS, but from the RTA and HAM as well. In addition, the radiances are corrected for Response Versus Scan angle (RVS) and the reflectance factor (ρ_{RTA}) is included. Note that φ_{xxx} refers to the HAM angle of incidence for the OBC, SVS, or BCS source (the RVS for the OBC is normalized to 1). The RVS used here was calculated by the NICST team.

Now we calculate the scan dependent, background subtracted source radiances, or

$$\Delta L_{OBC}\left(B,D,j_H,T_{OBC}\right) = \left\langle L_{OBC}\left|B,D,j_H,T_{OBC}\right.\right\rangle_{eff} - \left\langle L_{Bkg}\left|B,D,j_H,T_{OBC}\right.\right\rangle, \tag{6}$$

and

$$\Delta L_{BCS}\left(B,D,j_H,T_{BCS}\right) = \left\langle L_{BCS}\left|B,D,j_H,T_{BCS}\right.\right\rangle - \left\langle L_{Bkg}\left|B,D,j_H,T_{BCS}\right.\right\rangle. \tag{7}$$

In order to determine the radiometric gains, polynomial fits were conducted to the response versus the delta OBC radiance. Least-squares fits were performed over the dynamic range (F6) at the linear, quadratic, and cubic levels (or order N). These polynomials take the from

$$\Delta L_{OBC}\left(B,D,j_H,T_{OBC}\right) = \sum_{i=0}^{N} a_i dn_{OBC}^{i}\left(B,D,j_H,T_{OBC}\right). \tag{8}$$

This fitting is conducted on a scan by scan basis. The inverse of the linear term ($1/a_1$) is the radiometric gain.

Next, we need to calculate the retrieved calibration source radiance, or

$$\left\langle L_{OBC}\left| B,D,j_H,T_{OBC},N \right.\right\rangle_{ret} = \frac{\Delta L_{BCS}\left| B,D,j_H,T_{BCS} \right. \sum_{i=0}^{N} a_i dn^i_{OBC}\left| B,D,j_H,T_{OBC} \right.}{\sum_{i=0}^{N} a_i dn^i_{BCS}\left| B,D,j_H,T_{BCS} \right.} + \left\langle L_{Bkg}\left| B,D,j_H,T_{OBC} \right.\right\rangle \quad . \tag{9}$$

For the OBC source, we also determine the effective OBC emissivity. Here we use the following equation

$$\varepsilon_{OBC}\left| B,D,T_{OBC} \right. = \frac{\left\langle L_{OBC}\left| B,D,T_{OBC} \right.\right\rangle_{ret} - \left\langle L_{Bkg}\left| B,D,T_{OBC} \right.\right\rangle}{\left\langle L_{OBC}\left| B,D,T_{OBC} \right.\right\rangle - \left\langle L_{Bkg}\left| B,D,T_{OBC} \right.\right\rangle}, \tag{11}$$

where the retrieved OBC radiance and the background radiance were both averaged over scans and HAM sides. The emissivity is then averaged over detectors.

Note that the emissivity calculated in Equation (11) is not a prediction. As an input in Equation (4), the emissivity calculated by Equation (11) is a verification of this methodology.

3. Analysis

Now the results of RC-05 Part 2 for the nominal plateau are discussed. HAM sides A and B yield similar results. In consequence, only HAM side A is presented here, unless otherwise noted. In addition, only the warm-up and cool-down (RC-05 Part 2) radiometric gains are discussed. The specifications addressed here are listed in Table 2 [7]. The collects are referred to here by their collect label (see Table 1). The radiometric gains given here are for the F6 aperture.

Figure 1 shows the OBC temperature as a function of scan for both warm-up and cool-down (note that SRV0598 is satisfied during the warm-up portion). Figures 2 and 3 display the OBC temperature for each individual collect along with a straight line fit for warm-up and cool-down, respectively. In compliance with SRV0654, the temperature variation for warm-up is less than ±0.2 K.

The standard deviations for each of the six thermistors are shown in Figure 4 for both warm-up and cool-down. The average value per collect is given in Table 3. Due to the fact that all the warm-up collects vary less than 0.03 K, the requirement SRV0095 is satisfied.

The radiometric gains for both the warm-up and cool-down are listed in Table 4. Here the gains have been averaged over scans, subsample, and detector. The radiometric gains calculated from RC-05 Part 1 by NICST [1] are shown for comparison. The Part 2 warm-up gains agree with the NICST Part 1 (quadratic fit) gains to within 0.7% for all bands, except M12 and M13 hg which agree to within 1.2%. The difference for bands M12 and M13 hg is only 0.6% when the cubic fit is used for Part 1. As shown in [1], the fitting residual is greatly improved using a cubic fit for these bands and that the improvement occurs at low temperature. For Part 2, this low temperature region is not accessible and a

quadratic fit suffices. The cool-down gains show similar agreement, about 0.8% or less (using the quadratic fit for all bands). The warm-up gains are stable versus HAM side to approximately 0.8%; however, the cool-down gains are less stable, with a percent difference of 1.5% for all bands (except band I5 with 4%). Figure 5 plots of delta radiance vs dn for all bands and a middle detector (detector 8 for M bands and detector 16 for I bands) for both warm-up (black) and cool-down (red).

The coefficients from the quadratic fits (a_0, a_1, and a_2) are shown for both warm-up (black) and cool-down (red) in Figures 6, 7, and 8, respectively. There is a noticeable difference in the coefficients a_0 and a_2 between warm-up to cool-down whereas the coefficient a_1 is relatively stable (the exception is band I5). Here a_0 is the radiance offset, a_1 is the inverse of the gain, and a_2 is the nonlinear term.

Figure 9 plots of the percent difference between warm-up and cool-down for the coefficient a_1 for all bands and detectors. The percent difference between warm-up and cool-down a_1 is less than 3% (except for band I5 with 8%).

Detector 1 for band M14 was Out Of Family (OOF), as seen in Figure 5. The radiometric gains for this detector were computed using collects with OBC temperatures below 305 K. It was not included in the average show in Table 4.

Tables 5 and 6 list the individual detector gains for warm-up and cool-down, respectively. There is less than 14% variation as a function of detector for the warm-up and under 12% for the cool-down (expect for band I5 which has 17% and 20% variation, respectively). The variation between individual detectors from warm-up to cool-down is less than 7.0%. Figure 10 shows the radiometric gains as a function of detectors for warm-up (black) and cool-down (red).

The emissivity calculated using Equation (11) was 0.9966 and the input value in Equation (4) was 0.9983, a difference of about 0.2%. This gives us confidence that this methodology is accurate.

4. Summary

- The OBC temperature was controlled from ambient to 315 K (SRV0598).
- The OBC temperature was maintained at less than ±0.2 K of the programmed setpoint (SRV0654).
- The standard deviation of the OBC temperature over scans was less than 0.03 K for the warm-up (SRV0095).
- The radiometric gains for Part 2 (quadratic fit) are in good agreement with the results from Part 1 (quadratic fit, except for M12 and M13 hg with cubic fit).
- The warm-up gains were stable to less than 0.8% as a function of HAM side; the cool-down gains were stable to less than 1.5% as a function of HAM side (except band I5 with 4%).
- Noticeable difference between warm-up and cool-down for the radiance offset (a_0) and the nonlinear term (a_2).

- The inverse of the gain (a_1) is stable between warm-up and cool-down to within 3% (except band I5 with 8%).
- Large variation in individual detector gains within a given band.

Acknowledgement

The sensor test data used in this document was provided by the SBRS testing team. Approaches for data acquisition and data reductions, as well as data extraction tools were also provided by the SBRS. We would like to thank the SBRS team for their support. The data analysis tools were developed by the NICST team, and we would like to extend our gratitude for their valued assistance.

Table 1: EDU RC-05 Part 2 UAIDs with corresponding OBC and BCS temperatures.

UAID / Collect	Collect Label	OBC Temperature (K)	BCS Temperature (K)
2002542 / 1	1	272.6	299.9
2002542 / 2	2	282.6	299.9
2002542 / 3	3	292.6	299.9
2002542 / 4	4	297.7	299.9
2002542 / 5	5	302.7	299.9
2002542 / 6	6	307.7	299.9
2002543 / 1	7	312.7	299.9
2002543 / 2	8	315.2	299.9
2002544 / 1	9	312.0	299.9
2002544 / 2	10	307.2	299.9
2002544 / 3	11	302.2	299.9
2002544 / 4	12	297.2	299.9
2002544 / 5	13	292.3	299.9

Table 2: Specifications addressed by this work [7].

SRV0598	The sensor shall be capable of controlling the temperature of the on-board blackbody to a commamdable setpoint between approximately ambient and 315 K.
SRV0654	The sensor shall be capable of maintianing the temperature of the on-board blackbody to within ±0.2 K of the programmed setpoint temperature.
SRV0095	The emitting surface of the VIIRS sensor on-board blackbody source shall have a temperature uniformity of 0.03 K when operated under temperature controlled or unpowered conditions. Temperature uniformity is defined as the standard deviation of the temperatures measured by the sensors embbedded in the OBC BB.

Table 3: Average standard deviations for all 6 OBC thermistors.

OBC Temperature (K)	Thermistor Average Standard Deviation
272.6	0.00093
282.6	0.0025
292.6	0.0029
297.7	0.0047
302.7	0.0053
307.7	0.0039
312.7	0.0041
315.2	0.0033
312.0	0.22
307.2	0.19
302.2	0.16
297.2	0.13
292.3	0.11

Table 4: Detector, scan, and subsample averaged radiometric gains (F6) for HAM side A.

Band	RC-05 Part 1		RC-05 Part 2			
	NICST [1]		NICST			
			Warm up		Cool down	
	Gain (Quadratic)	Gain (Cubic)	Gain (Quadratic)	Standard Deviation	Gain (Quadratic)	Standard Deviation
I4	1104	1108	1100	31.7	1103	42.2
I5	104.6	104.7	104.2	9.55	104.0	33.2
M12	1751	1729	1730	32.4	1739	34.0
M13 hg	727.1	719.8	720.1	20.5	723.3	21.0
M14	243.9	242.4	245.6	41.0	245.8	38.1
M15	220.7	220.8	220.6	5.38	221.9	6.47
M16A	253.4	253.1	253.8	5.28	255.0	13.3
M16B	257.2	256.9	258.2	6.36	259.2	14.4

Table 5: Radiometric gains (F6) from the warm-up for HAM side A.

Detector	I4	I5	M12	M13 hg	M14	M15	M16A	M16B
1	1053	105.1	1708	723.5	344.7	224.7	253.9	262.4
2	1023	105.2	1698	716.0	252.4	220.7	259.9	261.4
3	1058	106.9	1750	746.0	237.9	224.8	252.6	257.9
4	1050	105.8	1716	719.7	237.9	223.1	255.2	262.1
5	1082	109.0	1769	750.3	241.5	226.8	256.0	260.5
6	1088	105.4	1713	716.1	248.6	211.4	261.4	263.8
7	1110	105.1	1770	742.2	247.3	228.2	254.4	264.8
8	1081	101.1	1724	709.2	243.3	224.7	262.6	267.8
9	1128	109.0	1774	743.5	233.5	222.4	249.9	259.4
10	1134	108.6	1731	716.2	237.7	221.2	255.4	253.9
11	1124	111.7	1750	745.1	232.0	223.8	250.1	260.4
12	1108	110.4	1774	707.7	242.6	219.0	254.4	254.3
13	1135	108.7	1740	716.8	244.8	213.0	252.0	254.2
14	1119	109.1	1695	684.9	239.5	216.5	252.5	252.4
15	1137	107.8	1702	704.2	226.3	219.8	246.8	250.5
16	1112	108.3	1661	680.6	218.8	209.6	244.6	244.8
17	1135	108.9	~	~	~	~	~	~
18	1148	106.2	~	~	~	~	~	~
19	1121	106.8	~	~	~	~	~	~
20	1113	104.8	~	~	~	~	~	~
21	1140	106.3	~	~	~	~	~	~
22	1089	101.2	~	~	~	~	~	~
23	1102	103.4	~	~	~	~	~	~
24	1092	103.7	~	~	~	~	~	~
25	1114	102.9	~	~	~	~	~	~
26	1099	99.23	~	~	~	~	~	~
27	1115	99.80	~	~	~	~	~	~
28	1072	97.60	~	~	~	~	~	~
29	1112	94.08	~	~	~	~	~	~
30	1062	95.81	~	~	~	~	~	~
31	1068	94.93	~	~	~	~	~	~
32	1059	93.02	~	~	~	~	~	~

Table 6: Radiometric gains (F6) from the cool-down for HAM side A.

Detector	I4	I5	M12	M13 hg	M14	M15	M16A	M16B
1	1052	106.2	1720	726.4	375.6	226.9	258.2	265.5
2	1027	103.9	1709	720.1	250.0	222.4	264.0	264.5
3	1061	102.0	1757	750.5	235.5	226.7	255.2	257.8
4	1051	106.2	1727	719.9	234.1	223.3	251.2	264.4
5	1084	107.1	1778	752.2	238.3	226.7	256.5	258.8
6	1093	107.0	1723	719.0	246.4	216.9	265.0	261.8
7	1112	104.1	1779	744.3	242.2	228.2	256.4	265.5
8	1084	107.1	1731	711.2	242.3	226.0	264.3	268.2
9	1134	114.9	1782	748.3	233.9	220.9	247.1	261.4
10	1134	109.4	1741	720.0	233.0	223.4	253.0	259.4
11	1131	110.4	1760	747.3	230.7	225.8	247.9	263.4
12	1112	108.9	1780	709.4	243.0	219.0	254.3	253.8
13	1135	107.1	1745	720.9	245.1	211.7	257.3	257.2
14	1121	106.1	1706	690.6	236.9	219.6	256.5	250.9
15	1138	115.9	1712	707.1	225.0	220.2	249.8	250.3
16	1115	109.1	1668	685.0	221.4	212.3	243.2	243.5
17	1138	110.9	~	~	~	~	~	~
18	1151	100.9	~	~	~	~	~	~
19	1126	107.9	~	~	~	~	~	~
20	1116	103.4	~	~	~	~	~	~
21	1144	106.9	~	~	~	~	~	~
22	1088	94.73	~	~	~	~	~	~
23	1106	101.3	~	~	~	~	~	~
24	1093	103.3	~	~	~	~	~	~
25	1119	102.2	~	~	~	~	~	~
26	1101	98.77	~	~	~	~	~	~
27	1126	94.71	~	~	~	~	~	~
28	1078	95.47	~	~	~	~	~	~
29	1115	98.05	~	~	~	~	~	~
30	1074	96.50	~	~	~	~	~	~
31	1072	92.74	~	~	~	~	~	~
32	1069	93.20	~	~	~	~	~	~

Figure 1: OBC temperature (K) as a function of scan and collect.

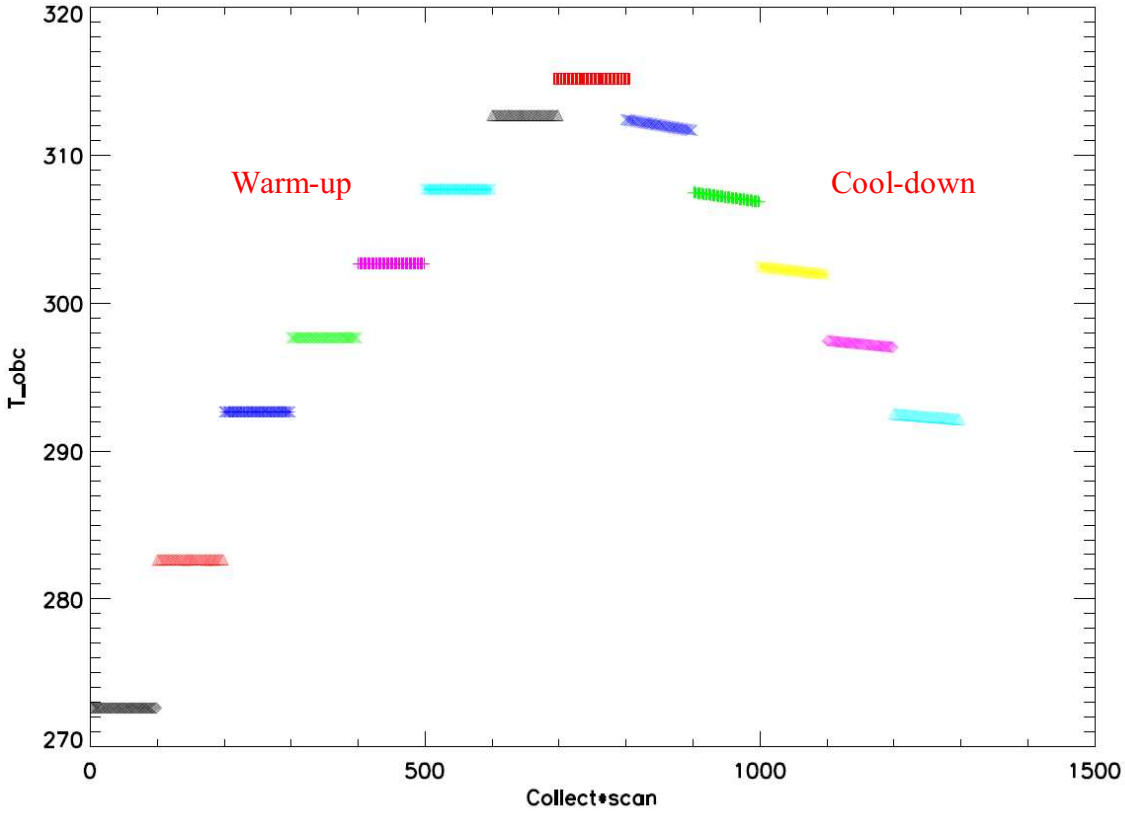

Figure 2: OBC temperature (K) as a function of scan for each warm-up collect.

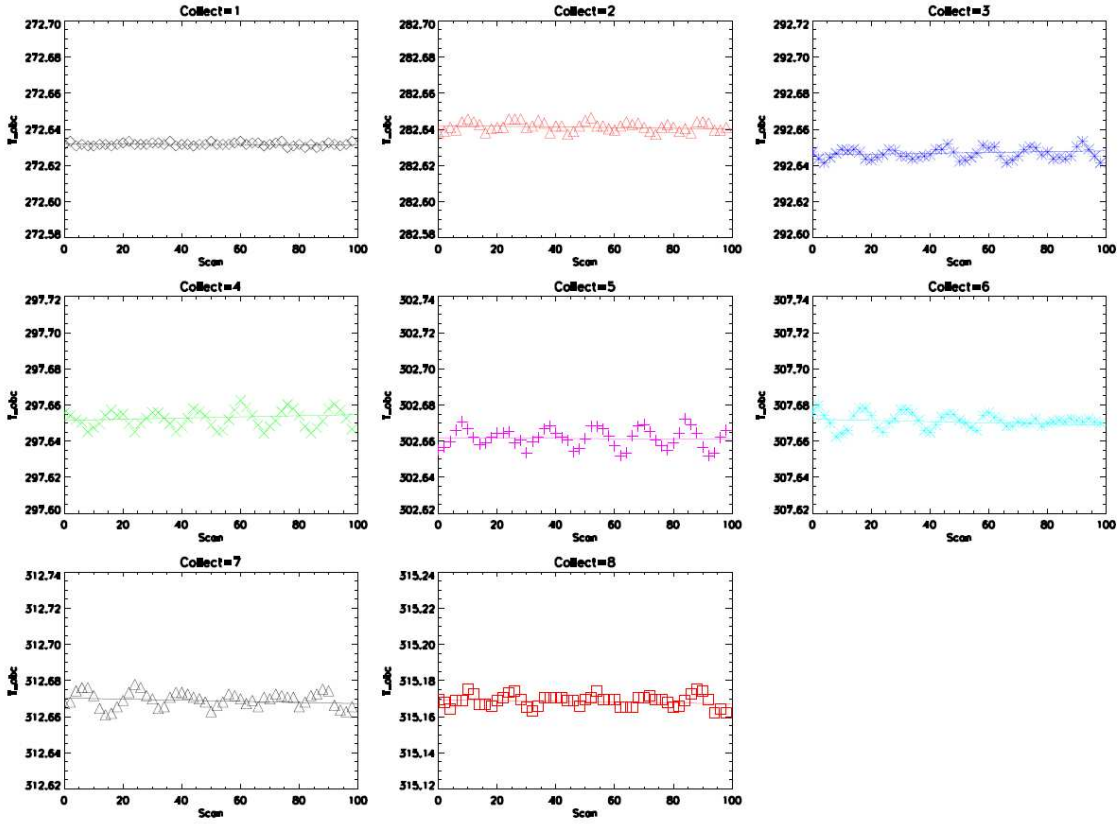

Figure 3: OBC temperature (K) as a function of scan for each cool-down collect.

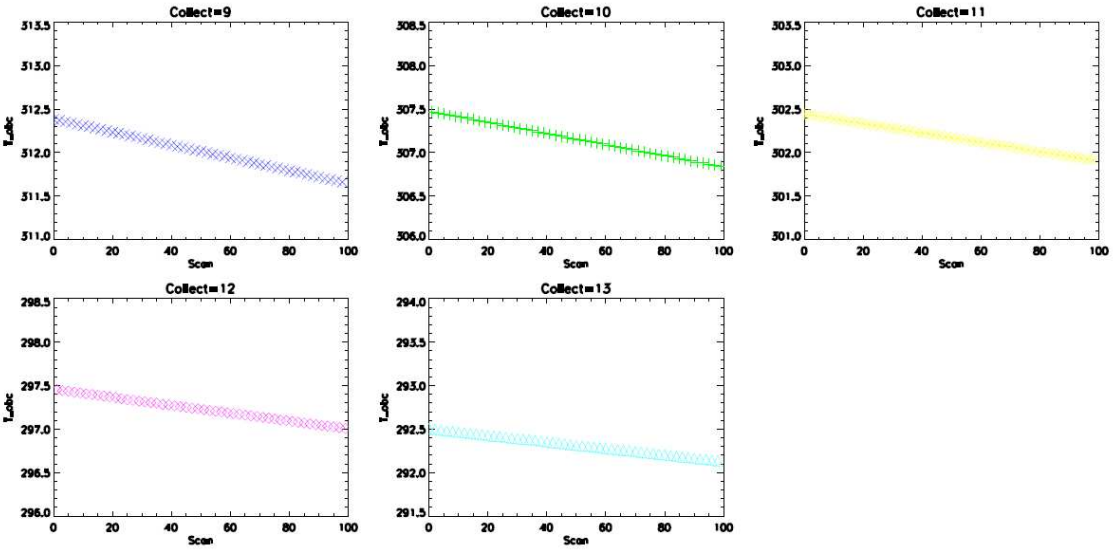

Figure 4: Standard deviation of OBC temperature for each thermistor as a function of collect.

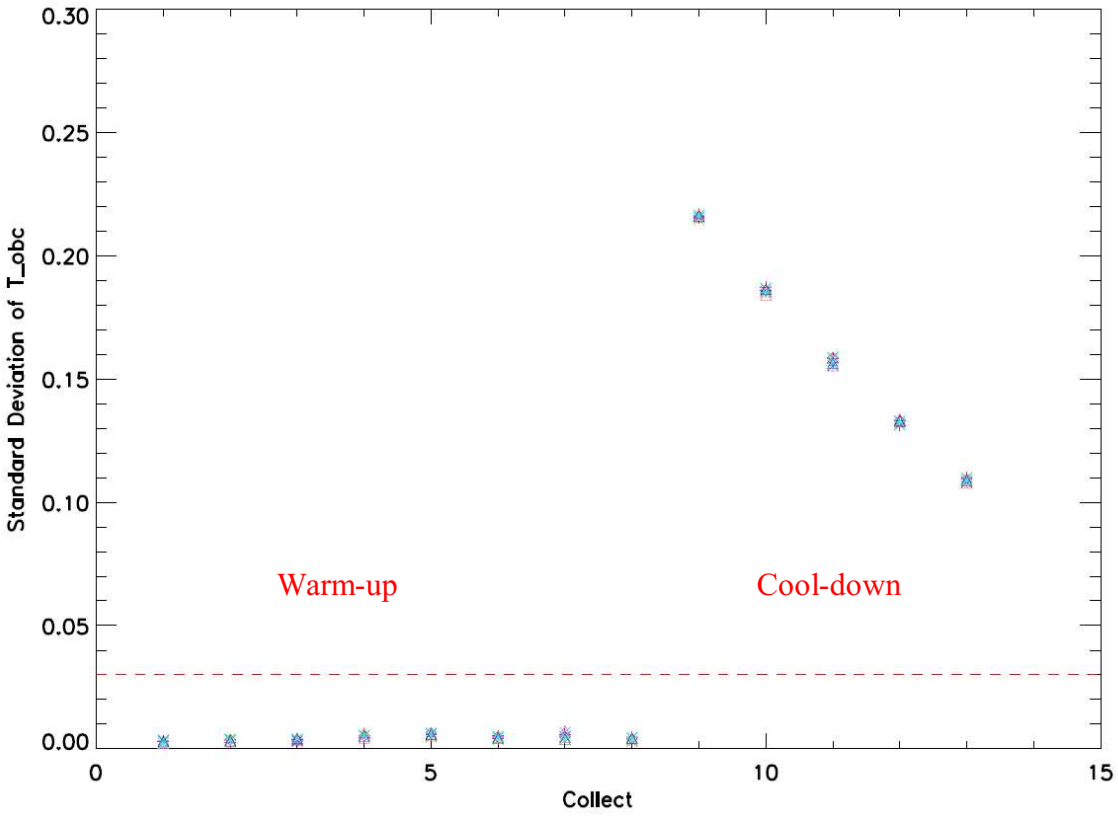

Figure 5: dn_{OBC} versus dL_{OBC} for the middle detectors (HAM side A and subsample 1). Detector 1 for band M14 is also included.

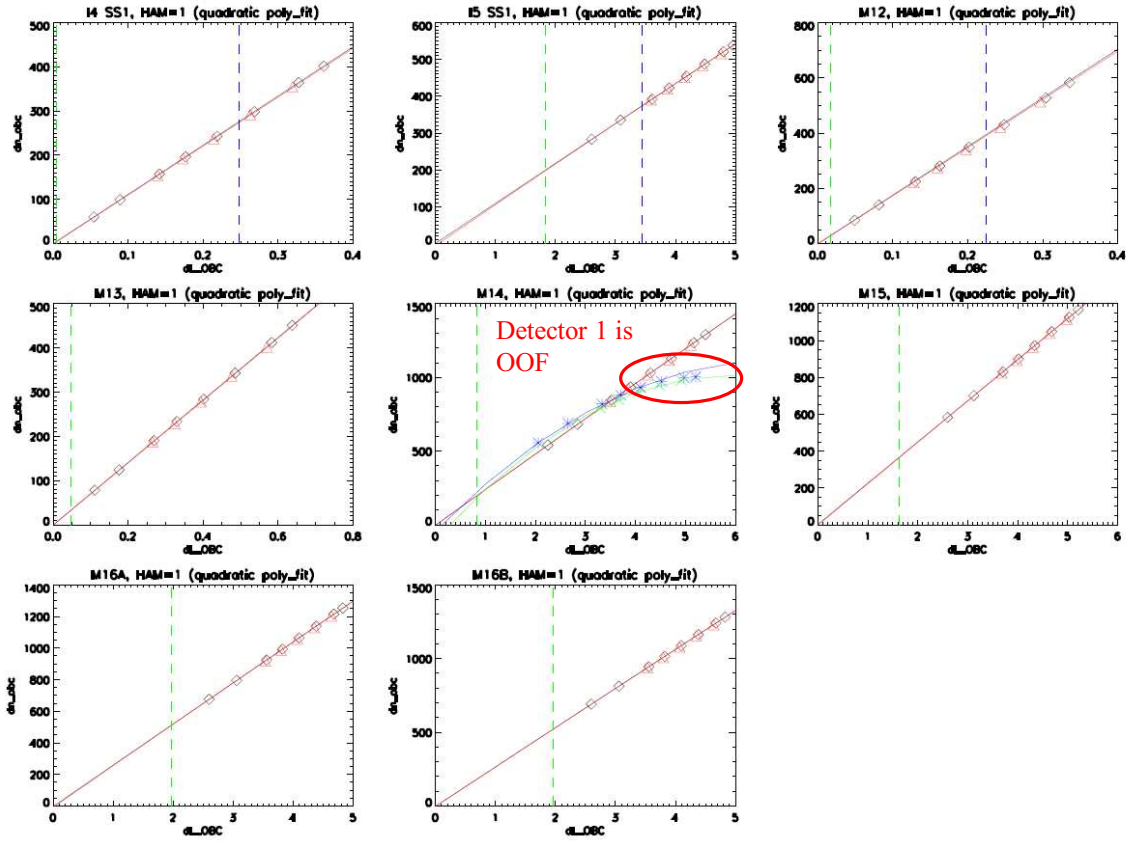

Figure 6: Warm-up and cool-down coefficient a_0 (F6) for each individual detector and band (HAM side A and subsample 1).

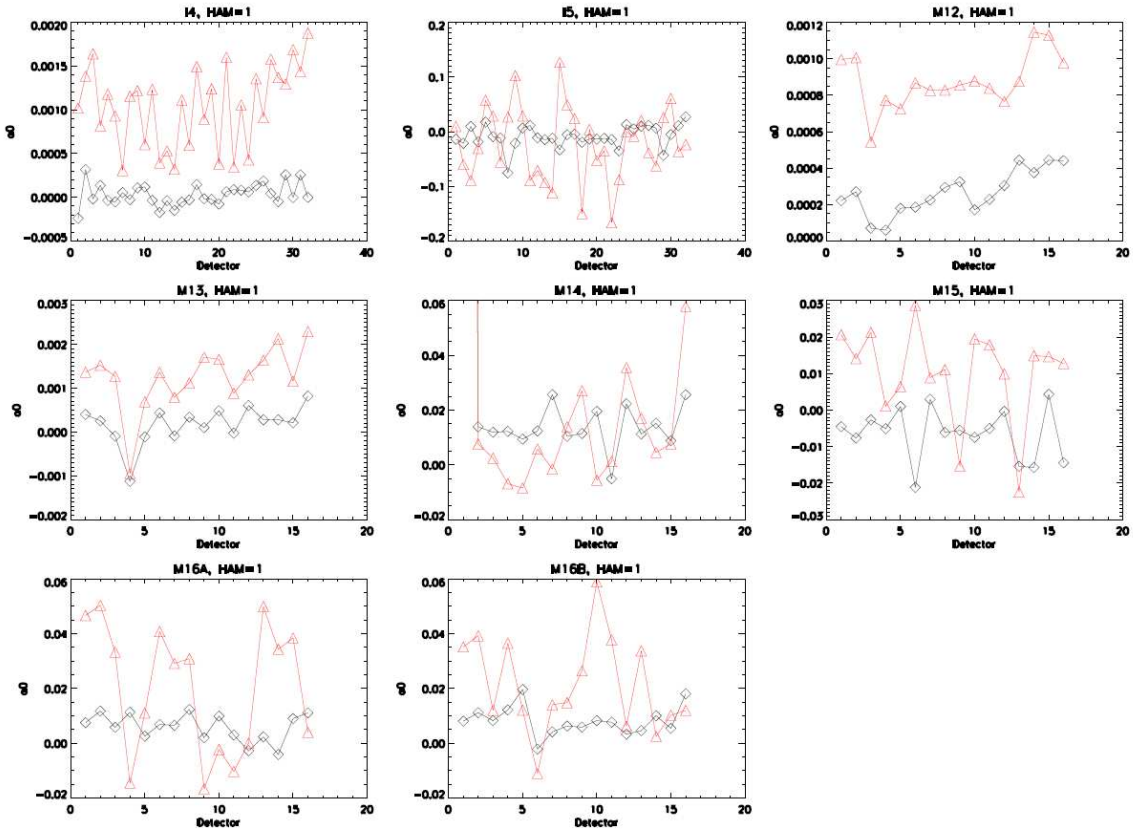

Figure 7: Warm-up and cool-down coefficient a_1 (F6) for each individual detector and band (HAM side A and subsample 1).

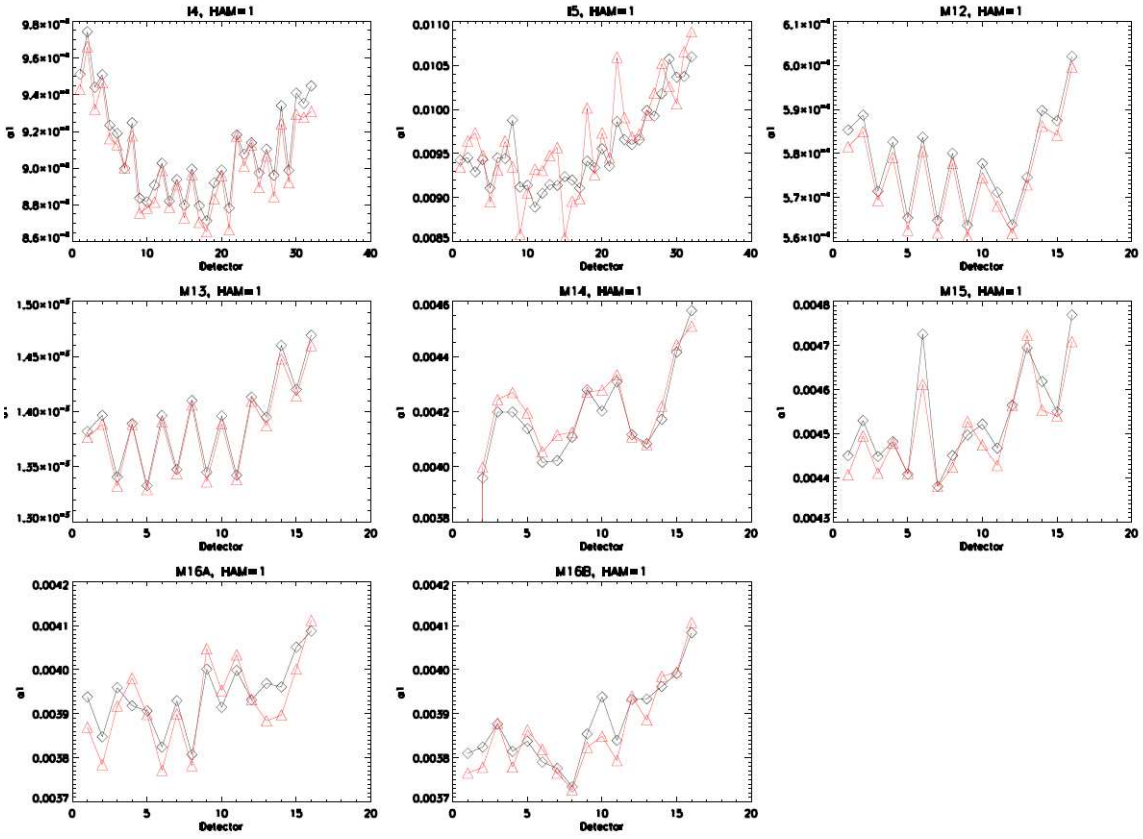

Figure 8: Warm-up and cool-down coefficient a_2 (F6) for each individual detector and band (HAM side A and subsample 1).

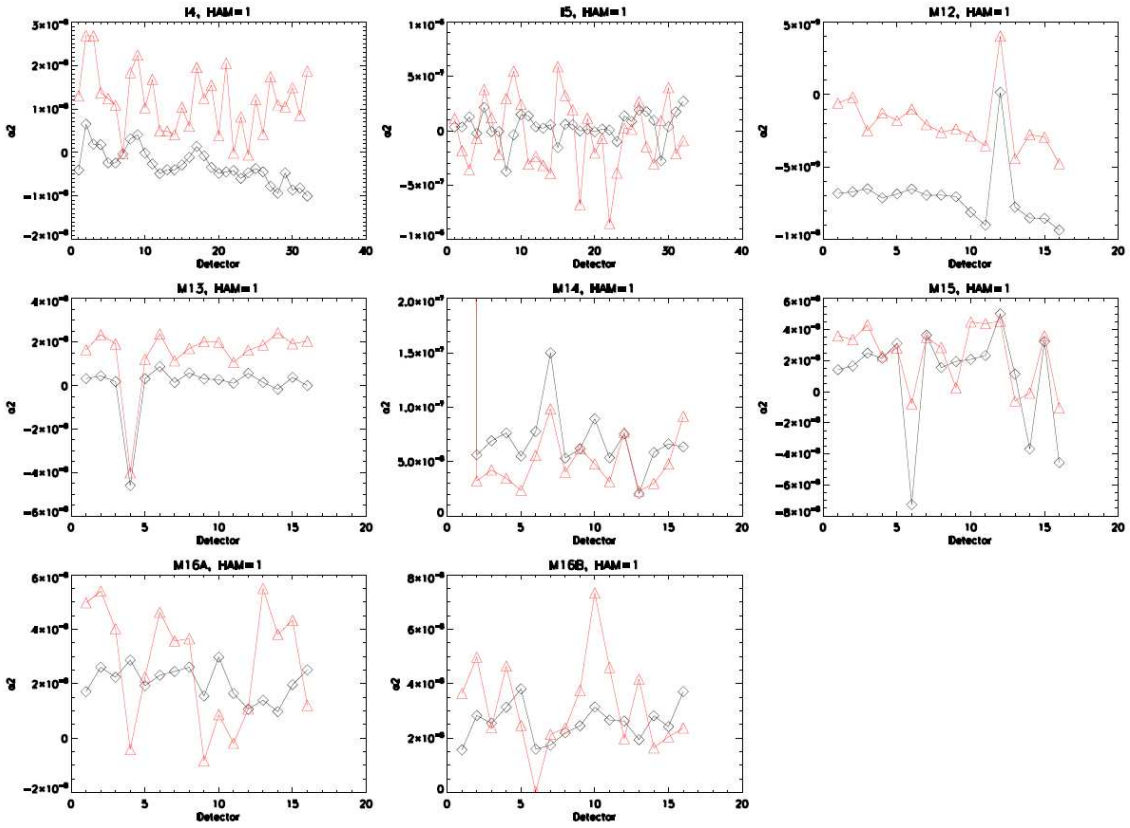

Figure 9: Percent difference in coefficient a_1 (F6) between warm-up and cool-down for each individual detector and band (HAM side A and subsample 1).

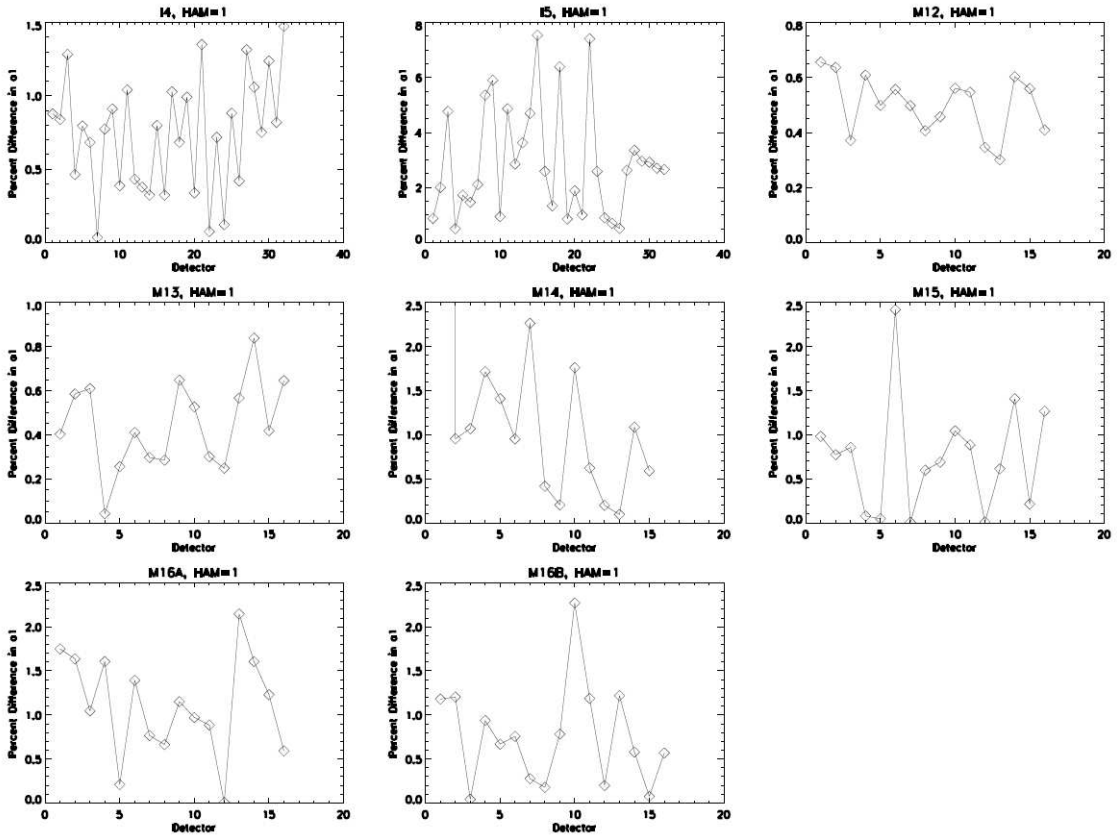

Figure 10: Radiometric gains (F6) for each individual detector and band (HAM side A and subsample 1).